

# Journal of Materials Chemistry A

Accepted Manuscript



This is an *Accepted Manuscript*, which has been through the Royal Society of Chemistry peer review process and has been accepted for publication.

*Accepted Manuscripts* are published online shortly after acceptance, before technical editing, formatting and proof reading. Using this free service, authors can make their results available to the community, in citable form, before we publish the edited article. We will replace this *Accepted Manuscript* with the edited and formatted *Advance Article* as soon as it is available.

You can find more information about *Accepted Manuscripts* in the [Information for Authors](#).

Please note that technical editing may introduce minor changes to the text and/or graphics, which may alter content. The journal's standard [Terms & Conditions](#) and the [Ethical guidelines](#) still apply. In no event shall the Royal Society of Chemistry be held responsible for any errors or omissions in this *Accepted Manuscript* or any consequences arising from the use of any information it contains.

1 **Novel PtCo alloy nanoparticles decorated 2D g-C<sub>3</sub>N<sub>4</sub> nanosheets with**  
2 **enhanced photocatalytic activity for H<sub>2</sub> evolution under visible light**  
3 **irradiation**

4 Changcun Han <sup>a, b</sup>, Yan Lu <sup>b</sup>, Junlong Zhang <sup>b</sup>, Lei Ge\* <sup>a, b</sup>, Yujing Li <sup>b</sup>,

5 Changfeng Chen <sup>b</sup>, Yongji Xin <sup>b</sup>, Linen Wu <sup>b</sup>, Siman Fang <sup>b</sup>

6 <sup>a</sup> State Key Laboratory of Heavy Oil Processing, College of Science, China University of Petroleum  
7 Beijing, No. 18 Fuxue Rd., Beijing 102249, People's Republic of China.

8 <sup>b</sup> Department of Materials Science and Engineering, College of Science, China University of Petroleum  
9 Beijing, No. 18 Fuxue Rd., Beijing 102249, People's Republic of China.

10 **Abstract**

11 Novel two-dimensional (2D) graphitic carbon nitride (g-C<sub>3</sub>N<sub>4</sub>) photocatalysts decorated with PtCo  
12 bimetallic alloy nanoparticles (NPs) were prepared via an in-situ chemical deposition method. The  
13 physical and chemical properties of the as-prepared PtCo/g-C<sub>3</sub>N<sub>4</sub> samples were characterized by  
14 X-ray diffraction (XRD), ultraviolet-visible diffuse reflection spectroscopy (DRS), transmission  
15 electron microscope (TEM), X-ray photoelectron spectroscopy (XPS) and surface photovoltage  
16 spectroscopy (SPV). The photocatalytic H<sub>2</sub> evolution experiments indicate that the PtCo alloy  
17 co-catalyst can effectively promote the separation efficiency of photo-generated charge carriers in  
18 g-C<sub>3</sub>N<sub>4</sub>, and consequently enhance the H<sub>2</sub> evolution activity. The 1.0 wt% PtCo/g-C<sub>3</sub>N<sub>4</sub> nanosheet  
19 catalyst shows the highest catalytic activity, and corresponding H<sub>2</sub> evolution rate is 960 μmol·h<sup>-1</sup>·g<sup>-1</sup>,  
20 which are enhanced by 2.9 times compared with that of pristine bulk Pt/g-C<sub>3</sub>N<sub>4</sub> (330 μmol·h<sup>-1</sup>·g<sup>-1</sup>)  
21 under visible light irradiation. The photocatalyst can keep stable and maintain catalytic activity after  
22 irradiated for 28 h. A possible photocatalytic mechanism of PtCo NPs on the enhancement of visible  
23 light performance is proposed to guide further improvement for other desirable functional materials.

1 **Keywords:** Water splitting; g-C<sub>3</sub>N<sub>4</sub> nanosheets; PtCo bimetallic alloy; Photocatalysis.

## 2 **1. Introduction**

3 Over the past few decades, semiconductor photocatalysis has drawn great attention due to its  
4 environmental and energy conversion application.<sup>1-8</sup> Graphitic carbon nitride (g-C<sub>3</sub>N<sub>4</sub>) is one of the  
5 most widely studied semiconducting materials with a number of advantageous characteristics including  
6 low cost, non-toxicity and superior photocatalytic activity.<sup>9-11</sup> Since the first discovery of its  
7 photocatalytic activity under visible light, g-C<sub>3</sub>N<sub>4</sub> has also been widely studied as a photocatalyst in  
8 applications such as water splitting,<sup>12, 13</sup> environmental purification<sup>14</sup> and CO<sub>2</sub> reduction.<sup>15</sup> Nevertheless,  
9 pure g-C<sub>3</sub>N<sub>4</sub> suffers from weakness such as low visible light utilization efficiency, a small specific  
10 surface area and rapid recombination of photo-generated charge carriers.<sup>16-18</sup> In order to solve the above  
11 problems, two approaches have been employed to enhance the visible light photocatalytic  
12 performance of g-C<sub>3</sub>N<sub>4</sub>: (i) exfoliation into two-dimensional structure,<sup>19-21</sup> (ii) doping with metals or  
13 surface coupling hybridization.<sup>22, 23</sup>

14 In general, bulk g-C<sub>3</sub>N<sub>4</sub> photocatalysts are still exhibit relatively low photocatalytic activity  
15 because of multilayer gathered to form large objects with less surface active areas. In order to increase  
16 the surface area of g-C<sub>3</sub>N<sub>4</sub>, great efforts have recently been devoted to preparing g-C<sub>3</sub>N<sub>4</sub> nanosheets and  
17 investigating their photocatalytic performance.<sup>20, 21</sup> For instance, g-C<sub>3</sub>N<sub>4</sub> nanosheets can be obtained by  
18 liquid exfoliation bulk g-C<sub>3</sub>N<sub>4</sub> in water,<sup>20</sup> methanol solution<sup>24</sup> and concentrated sulfuric acid et al.<sup>19</sup>  
19 Unfortunately, most of the current methods to fabricate g-C<sub>3</sub>N<sub>4</sub> nanosheets are usually time consuming  
20 or low yield. Recently, a facile one step method for realizing scalable production of g-C<sub>3</sub>N<sub>4</sub> nanosheets  
21 were reported.<sup>25</sup> This method offers the superiority of low cost, scalable production and high efficiency,  
22 and could increase the surface area in a controllable manner while still no inhibition the activity of per  
23 unit area, and therefore achieve enhanced photocatalytic activity. However, the g-C<sub>3</sub>N<sub>4</sub> nanosheets still

1 suffer from the fast recombination of charge carriers in the photocatalytic process.

2 When metals and g-C<sub>3</sub>N<sub>4</sub> semiconductors are in contact, because of the lower Fermi levels of  
3 precious metals, metals can act as an electron capturer suppressing the recombination, thus extending  
4 the lifetime of charge carriers and significantly enhancing the activity of photocatalytic redox  
5 reactions.<sup>26,27</sup> Among the noble metals, Pt is considered the best candidate for photocatalytic hydrogen  
6 evolution due to its high work function. Compared to monometallic NPs, bimetallic NPs show greater  
7 potential in catalytic applications due to their unique microstructures and enhanced catalytic  
8 performance. Bimetallic catalytic systems can potentially achieve chemical transformations that can  
9 hardly be accomplished by monometallic catalysts, which can be attributed to the reason that different  
10 components of the catalysts have a particular function in the reaction mechanism.<sup>28,29</sup> It is observed that  
11 the activity, selectivity and resistance to poisoning of the metal catalysts can be drastically influenced by  
12 the presence of a second metal component.<sup>30</sup> In our previous work, we found that the AuPd NPs has  
13 higher H<sub>2</sub> catalytic activity than single noble metal.<sup>31</sup> Compared with pure Pt, Pt-based transition metal  
14 alloys exhibit higher activity in many reactions. For instance, it was reported that higher oxygen  
15 reduction reaction (ORR) activity could be achieved by alloying Pt with several transition metals such  
16 as Fe, Co and Ni.<sup>32-34</sup>

17 In this study, for the first time we have developed a novel photocatalyst by loading PtCo bimetallic  
18 alloy on g-C<sub>3</sub>N<sub>4</sub> nanosheets via an ethylene glycol reduction method. The activity of g-C<sub>3</sub>N<sub>4</sub> can be  
19 significantly enhanced by adding the mono-dispersed PtCo co-catalyst NPs. The 1.0 wt% PtCo/g-C<sub>3</sub>N<sub>4</sub>  
20 shows the highest H<sub>2</sub> evolution activity of 960 μmol·h<sup>-1</sup>·g<sup>-1</sup>, which is 2.9 times higher than that of bulk  
21 1.0 wt% Pt/g-C<sub>3</sub>N<sub>4</sub>. The effects of PtCo on the visible light absorption, charge transfer process and  
22 photocatalytic activity were investigated in detail, and the catalytic mechanism for the enhanced H<sub>2</sub>  
23 evolution activity was also discussed. This work may provide more insight into synthesizing novel

1 Pt-based alloy co-catalysts materials with high activities for applications into solar energy conversion  
2 and utilization.

## 3 **2. Experimental**

### 4 **2.1 synthesis of PtCo/g-C<sub>3</sub>N<sub>4</sub> catalyst**

5 All chemical were reagent grade and without used further purification. The g-C<sub>3</sub>N<sub>4</sub> nanosheets bulk  
6 were prepared by heating 4g cyanamide and 10g ammonium chloride in a crucible with cover to 550 °C  
7 for 4h at a heating rate of 4 °C/min. A light yellow powder of g-C<sub>3</sub>N<sub>4</sub> was obtained. The PtCo alloy NPs  
8 were prepared according to references with slight modification.<sup>35</sup> The PtCo alloy was synthesized via  
9 the reduction of Pt and Co salts together in ethylene glycol (EG). All of the EG solution was to adjust  
10 pH=11.5 by NaOH solution. In a typical experiment, 1g/L (Pt) H<sub>2</sub>PtCl<sub>6</sub> and 1g/L (Co) CoCl<sub>2</sub> EG  
11 solutions were prepared at stock solutions. The mixture was stirred for 30 min to form a homogeneous  
12 and light green solution. Then, a certain amount of g-C<sub>3</sub>N<sub>4</sub> was added to the above solution followed by  
13 magnetic stirring for 30 min and ultrasonic dispersion 30 min to form a homogeneous suspension. The  
14 solution was then transferred to the 50 ml Teflon-lined stainless steel autoclave and heated at 200 °C for  
15 10 h.

16 For comparison, we further adjusted the molar ratio of Pt to Co in the PtCo bimetallic alloy, and  
17 prepared a series of samples, including Pt/g-C<sub>3</sub>N<sub>4</sub>, Pt<sub>3</sub>Co/g-C<sub>3</sub>N<sub>4</sub>, PtCo/g-C<sub>3</sub>N<sub>4</sub>, PtCo<sub>3</sub>/g-C<sub>3</sub>N<sub>4</sub>,  
18 PtCo<sub>6</sub>/g-C<sub>3</sub>N<sub>4</sub>, Co/g-C<sub>3</sub>N<sub>4</sub>. The loading amounts of alloys in the g-C<sub>3</sub>N<sub>4</sub> are all controlled at 1.0 wt%. In  
19 order to investigate the different loading on the catalytic activity, The photocatalytic system loading  
20 amount of the PtCo were 0.1 wt% , 0.3 wt% , 0.5wt% , 1.0 wt% , 3.0wt% and 5.0 wt%, respectively.

### 21 **2.2 Characterization**

22 The crystal structure of the sample was investigated using X-ray diffraction (XRD; Bruker D8  
23 Advance) with CuK $\alpha$  radiation at a scan rate of 4min<sup>-1</sup>. The acceleration voltage and the applied current

1 were 40 kV and 40 mA, respectively. The morphology of the samples was examined by high resolution  
2 transmission electron microscopy (HR-TEM, FEI Tecnai G<sup>2</sup> F20; accelerating voltage=200kV). UV-Vis  
3 diffuse reflection spectroscopy (DRS) was performed on a Shimadzu UV-4100 spectrophotometer using  
4 BaSO<sub>4</sub> as the reference material. The X-ray photoelectron spectroscopy (XPS) was measured in a PHI  
5 5300 ESCA system. The beam voltage was 3.0 eV, and the energy of Ar ion beam was 1.0 keV. The  
6 binding energies were normalized to the signal for adventitious carbon at 284.8 eV.

### 7 **2.3 Photocatalytic activity**

8 The photocatalytic H<sub>2</sub> evolution experiments were performed in Perfect light Labsolar IIIAG  
9 system with a 300 ml quartz reactor. The reactor is connected to a low-temperature thermostat bath at 4  
10 °C. PLS-SXE 300C Xe arc lamp with a UV-cutoff (≥400nm) filter was used as the light source. The  
11 light intensity employed was 35mW/cm<sup>2</sup>. In a typical photocatalytic experiment, 50 mg of photocatalyst  
12 powder was suspended in a 100 mL of aqueous solution containing 10 vol.% triethanolamine (TEOA).  
13 Before photocatalytic experiments, the reaction vessel was evacuated for 30 min to remove the  
14 dissolved oxygen and to ensure the anaerobic conditions. The products were analyzed by  
15 chromatography (Beifen 3420A, high purity Argon as a carrier gas, 99.999%) equipped with a thermal  
16 conductivity detector.

### 17 **2.4. SPV measurements**

18 The surface photovoltage (SPV) measurement was carried out on a surface photovoltage  
19 spectroscopy (PL-SPS/IPCE1000 Beijing Perfect Light Technology Co., Ltd).<sup>36</sup> The measurement  
20 system consists of a source of monochromatic light, a lock-in amplifier (SR830, Stanford research  
21 systems, inc.) with a light chopper (SR540, Stanford research systems, inc.), and a sample chamber. The  
22 monochromatic light is provided by passing light from a 500 W Xenon lamp (CHFXQ500 W, global  
23 Xenon lamp power) through a grating mono-chromator (Omni-5007, No.09010, Zolix), which chopped

1 with a frequency of 24 Hz. All the measurements were operated at room temperature and under ambient  
2 pressure.

### 3 **3. Results and discussion**

#### 4 **3.1. Characterization of PtCo/g-C<sub>3</sub>N<sub>4</sub> composite samples**

5 The overall fabrication procedures of the PtCo/g-C<sub>3</sub>N<sub>4</sub> photocatalysts are schematically illustrated  
6 in Fig.1. The bulk g-C<sub>3</sub>N<sub>4</sub> was prepared via the reported method of our group.<sup>37,38</sup> The metal-free bulk  
7 g-C<sub>3</sub>N<sub>4</sub> powders were prepared through the heating melamine in an alumina combustion boat to 550°C  
8 for 4h at a heating rate of 2 °C /min. However, g-C<sub>3</sub>N<sub>4</sub> nanosheets were obtained by heating a mixture of  
9 melamine and ammonium chloride at 550 °C for 4h. With the increase of temperature, melamine was  
10 gradually polymerized, at the same time NH<sub>4</sub>Cl was decomposed into ammonia and hydrogen chloride  
11 gases, which inhibit the aggregation of melamine and resulted in 2D g-C<sub>3</sub>N<sub>4</sub> nanosheets. After PtCo  
12 bimetallic NPs loaded on the surface of g-C<sub>3</sub>N<sub>4</sub> nanosheets, the PtCo/g-C<sub>3</sub>N<sub>4</sub> nanosheets samples were  
13 obtained.

14 The X-ray diffraction patterns of the pristine and modified g-C<sub>3</sub>N<sub>4</sub> are shown in Fig.2. Typically,  
15 the pure g-C<sub>3</sub>N<sub>4</sub> nanosheets have two distinct peaks at 13.1° and 27.4°, which can be indexed as (1 0 0)  
16 and (0 0 2) peaks in JCPDS 87-1526. These two diffraction peaks are in good agreement with the  
17 g-C<sub>3</sub>N<sub>4</sub> reported in the literature.<sup>39,40</sup> However, no diffraction peaks corresponding to PtCo co-catalysts  
18 can be observed in Fig.2. This may be due to the small amount of PtCo NPs contents and highly  
19 dispersion in the polymeric g-C<sub>3</sub>N<sub>4</sub> photocatalysts. In order to better understand the nature of the PtCo  
20 “alloy” particle, we have added a series of pure PtCo<sub>x</sub> to support this conclusion. From the Fig.2b XRD  
21 inset, the pure Pt (JCPDS, No. 65-2868) XRD patterns exhibit diffraction peaks at approximately 39.7°  
22 (1 1 1) and 46.2° (2 0 0). After introducing Co element to PtCo<sub>x</sub> NPs, the diffraction peaks gradually  
23 moves to the right side. This result indicates that the as-prepared NPs are homogeneous PtCo bimetallic

1 alloys.

2 The UV-vis diffuse reflectance spectra (DRS) of as-prepared PtCo/g-C<sub>3</sub>N<sub>4</sub> samples were  
3 investigated and shown in Fig.3. The pure g-C<sub>3</sub>N<sub>4</sub> nanosheets shows absorption from the UV through  
4 the visible range up to 470 nm, the steep of the spectrum indicates that the visible light absorption is  
5 ascribed to the band gap transition, corresponding to a band gap of 2.6 eV for pure g-C<sub>3</sub>N<sub>4</sub>. After  
6 inducing PtCo NPs, the PtCo/g-C<sub>3</sub>N<sub>4</sub> sample show the similar absorption edge in shape and enhanced  
7 light absorption compared with pure g-C<sub>3</sub>N<sub>4</sub>. Fig.3a illustrates that the absorption intensities of the  
8 as-prepared samples are gradually strengthened with increasing Pt percentage in the PtCo<sub>x</sub> NPs in the  
9 visible light region. Fig.3b shows that the absorption intensities of the as-prepares samples are  
10 strengthened with increasing PtCo NPs contents, which agrees with the color of the prepared samples  
11 that vary from yellow to gray. The DRS results also indicate that the chemical deposited PtCo NPs  
12 could improve the visible light absorption, and hence is expected to increase photocatalytic  
13 performance.

14 The morphology and microstructure of the 1.0 wt% PtCo/g-C<sub>3</sub>N<sub>4</sub> nanosheets photocatalyst were  
15 investigated by TEM. Fig.4 displays the TEM and HRTEM images of PtCo/g-C<sub>3</sub>N<sub>4</sub> composites. As  
16 shown in Fig.4a, the g-C<sub>3</sub>N<sub>4</sub> samples consist of irregular ultrathin nanosheets. The Fig.4b and c  
17 illustrates the microstructures of composite samples, the g-C<sub>3</sub>N<sub>4</sub> nanosheets with PtCo NPs can be  
18 found. The PtCo NPs co-catalysts are decorated on the surface of g-C<sub>3</sub>N<sub>4</sub> to nanosheets form intimate  
19 interfaces facilitating charge transfer between the semiconductors; hence it is expected to improve the  
20 separation of photogenerated charge carriers and therefore the photocatalytic activity. As shown in  
21 Fig.4d, the PtCo NPs has diameters of 3-5nm and their crystallinity can be resolved. The lattice  
22 spacings measured for the crystalline planes are 0.218 nm, corresponding to the (1 1 1) plane of PtCo  
23 alloys (JCPDS 43-1358).

1 X-ray photoelectron spectrum (XPS) is used to investigate the valence states and chemical  
2 environment of constituent elements on the surface of the samples. The sample for XPS is 1.0 wt%  
3 PtCo/g-C<sub>3</sub>N<sub>4</sub> nanosheets. The survey XPS spectrum shows that the main elements on the surface of the  
4 product are C, N and small amount of Pt and Co. Fig.5a and b presents the high-resolution XPS spectra  
5 of C1s and N1s in the PtCo/g-C<sub>3</sub>N<sub>4</sub> sample. The C1s shows two distinct peaks at 284.8 and 288.2 eV.  
6 The first peak can be ascribed to carbon species adsorbed on the surface of photocatalysts; the second  
7 binding energy peak belongs to carbon atoms in g-C<sub>3</sub>N<sub>4</sub>. The N1s XPS binding energy can be divided  
8 into three peaks located at 398.53, 399.13 and 400.58 eV, which represent nitrogen atoms in the C=N-C,  
9 N-(C)<sub>3</sub> and C-N-H functional groups in the polymeric g-C<sub>3</sub>N<sub>4</sub> structures.<sup>39, 40</sup> As shown in Fig.5c, the Pt  
10 4f<sub>7/2</sub> and Pt 4f<sub>5/2</sub> peaks in the spectrum of Pt locate at 71.38 and 74.73 eV, respectively, which exhibit  
11 slight upshift as compared to pure Pt NPs.<sup>41</sup> In order to further verify the valence states of PtCo<sub>x</sub> alloys,  
12 the Pt, Pt<sub>3</sub>Co, PtCo and PtCo<sub>3</sub> samples were examined by XPS technique. Obviously, after Pt form alloy  
13 with Co, the Pt 4f binding energy of the Pt-Co bimetallic crystals shifted to right side compared to that  
14 of pure Pt NPs. The positions of Pt 4f<sub>7/2</sub> are 71.38, 71.53, 71.68 and 71.83 eV for Pt, Pt<sub>3</sub>Co, PtCo and  
15 PtCo<sub>3</sub>, respectively. The Co 2p<sub>3/2</sub> peak is about 778.2 eV, indicating the presence of bimetallic alloy.<sup>42</sup>  
16 The electronic structures of PtCo NPs are modified due to the alloying of Pt with Co.<sup>43, 44</sup>

### 17 **3.2 Photocatalytic H<sub>2</sub> evolution activity**

18 As shown in Fig.6, pure Pt/g-C<sub>3</sub>N<sub>4</sub> bulk sample shows obvious visible light photocatalytic activity  
19 with H<sub>2</sub> evolution rate of 330 μmol·g<sup>-1</sup>·h<sup>-1</sup>, which can be attributed to the moderate band gap and unique  
20 electronic of Pt/g-C<sub>3</sub>N<sub>4</sub>. After addition of a small amount of PtCo<sub>x</sub> NPs, the photocatalytic activity of  
21 PtCo<sub>x</sub>/g-C<sub>3</sub>N<sub>4</sub> is improved. The activity of the composite samples is further enhanced with higher Co  
22 contents. The bulk 1.0 wt% PtCo/g-C<sub>3</sub>N<sub>4</sub> sample shows the highest H<sub>2</sub> evolution rate of 689  
23 μmol·g<sup>-1</sup>·h<sup>-1</sup>, which is about 2.1 folds higher than that of pure bulk Pt/g-C<sub>3</sub>N<sub>4</sub>. A further increase in Co

1 content causes a decrease in the photocatalytic H<sub>2</sub> evolution. We propose that the origin of this effect is  
2 attributed to the reason that the PtCo bimetallic alloys have an appropriate mole ratio.

3 Compared to Fig.6, Fig.7 has a superior photocatalytic H<sub>2</sub> evolution activity when bulk g-C<sub>3</sub>N<sub>4</sub> is  
4 replaced by g-C<sub>3</sub>N<sub>4</sub> nanosheets. After introducing Pt nanoparticles, the intimate interfaces between Pt  
5 and g-C<sub>3</sub>N<sub>4</sub> are formed. It was reported that the high activity Pt can accept electrons and serve as active  
6 sites for hydrogen production. With increase of the Co content in the PtCo bimetallic alloy, the  
7 photocatalytic hydrogen evolution on PtCo<sub>x</sub>/g-C<sub>3</sub>N<sub>4</sub> is further enhanced. The PtCo/g-C<sub>3</sub>N<sub>4</sub> nanosheets  
8 sample shows the highest H<sub>2</sub> evolution rate of 960 μmol·g<sup>-1</sup>·h<sup>-1</sup>, which is about 1.34 folds higher than  
9 that of pure Pt/g-C<sub>3</sub>N<sub>4</sub> nanosheets (716 μmol·g<sup>-1</sup>·h<sup>-1</sup>).

10 To further investigate the catalytic activity of 2D nanosheet and bulk structures, the photocatalytic  
11 activities of bulk and nanosheet samples were conducted and compared. Fig.8 illustrates the rate of H<sub>2</sub>  
12 evolution over different bulk and nanosheet samples. After bulk materials are replaced by nanosheets,  
13 the catalytic activities are significantly enhanced. As shown in the Fig.8, the PtCo/g-C<sub>3</sub>N<sub>4</sub> nanosheet  
14 sample shows the highest photocatalytic performance with H<sub>2</sub> evolution rate of 960 μmol·h<sup>-1</sup>·g<sup>-1</sup>, about  
15 2.9 times higher than of bulk Pt/g-C<sub>3</sub>N<sub>4</sub> (330 μmol·h<sup>-1</sup>·g<sup>-1</sup>), which indicates that the nanosheets play an  
16 important role in enhancement of H<sub>2</sub> evolution activity in the PtCo/g-C<sub>3</sub>N<sub>4</sub> composite photocatalysts.

17 Fig.9 presents the H<sub>2</sub> evolution over PtCo/g-C<sub>3</sub>N<sub>4</sub> nanosheets photocatalysts with different PtCo  
18 NPs contents. After introducing 0.1wt% of PtCo NPs, the catalytic activity of H<sub>2</sub> evolution is  
19 significantly increased to 458.7 μmol·g<sup>-1</sup>·h<sup>-1</sup>. With continue to increase the PtCo NPs amount; the H<sub>2</sub>  
20 evolution rate over g-C<sub>3</sub>N<sub>4</sub> nanosheets is further enhanced. The 1.0 wt% sample shows the highest  
21 photocatalytic H<sub>2</sub> evolution rate of 960 μmol·g<sup>-1</sup>·h<sup>-1</sup>. However, a further increase of PtCo NPs contents  
22 lead to a slightly decrease of H<sub>2</sub> evolution. As a consequence, the 1.0 wt% PtCo/g-C<sub>3</sub>N<sub>4</sub> presents the  
23 best H<sub>2</sub> evolution activity in this study.

1 Besides activity, the stability of a photocatalyst is important for practical application. To  
2 demonstrate the stability of PtCo/g-C<sub>3</sub>N<sub>4</sub> nanosheets catalyst, we performed the cycled hydrogen  
3 evolution experiment over 1.0 wt% samples under the same conduction. Fig.10 presents the H<sub>2</sub>  
4 evolution curve in cycling photocatalytic runs. This results show that the composite sample display no  
5 obvious decrease of H<sub>2</sub> production activity after irradiated for 28 h, indicating that the PtCo/g-C<sub>3</sub>N<sub>4</sub>  
6 nanosheet sample has excellent stability for photocatalytic H<sub>2</sub> production.

### 7 3.3 Photocatalytic mechanism discussion

8 Based on the experimental results, we try to explain the photocatalytic mechanism of PtCo<sub>x</sub>/g-C<sub>3</sub>N<sub>4</sub>.  
9 The binary alloys show different structures and electronic density of states when compared with single  
10 metal, resulting in adjustable degeneration of physical chemical properties and surface states of PtCo<sub>x</sub>  
11 NPs. The “synergistic effect” of alloy elements will affect the Fermi energy level of the PtCo<sub>x</sub> alloys.  
12 As shown in Fig.11, the Fermi energy levels of PtCo<sub>x</sub> alloys are lower than that of g-C<sub>3</sub>N<sub>4</sub> conduction  
13 band, which makes the photo-excited electrons transfer from CB of g-C<sub>3</sub>N<sub>4</sub> to surface of PtCo<sub>x</sub> alloys  
14 and leads to efficient separation of electron-hole pairs. In the PtCo<sub>x</sub> alloys, the “synergistic effect” of Pt  
15 and Co elements makes the surface defects increase, and changes the Fermi energy level position in  
16 comparison to Pt (Fig.11). It is assumed that the transfer driving force may increase for photo-excited  
17 electrons from CB of g-C<sub>3</sub>N<sub>4</sub> to the PtCo alloy after introducing Co element. Hence, introduction of Co  
18 element is more beneficial to the capturing ability of photo-excited electrons in the PtCo<sub>x</sub> alloys, and  
19 enhance the photocatalytic activity. However, at the same time, the Co element decreases the active  
20 sites of H<sub>2</sub> evolution, because H<sup>+</sup> in solution is much easier to be adsorbed on the surface of Pt than that  
21 of Co.<sup>35</sup> The higher Co contents in PtCo<sub>x</sub> alloys may inhibit the adsorption of H<sup>+</sup> and decrease the  
22 activity in the PtCo<sub>x</sub>/g-C<sub>3</sub>N<sub>4</sub> samples. Therefore, for the H<sub>2</sub> evolution activity, introduction of Co to  
23 form PtCo<sub>x</sub> alloys has two influencing aspects: (1) it improves capturing ability of photo-excited

1 electrons; (2) it reduces active sites of H<sub>2</sub> production. Based on our results, H<sub>2</sub> evolution activity  
2 increases when Co is added into PtCo<sub>x</sub> alloys at the beginning, because the factor (1) is more effective  
3 than the factor (2). However, the activity decreases when more Co is introduced as the factor (2) is more  
4 dominant (as shown in Fig.8). The optimum ratio of Pt to Co is determined to be 1:1. Therefore, the  
5 PtCo/g-C<sub>3</sub>N<sub>4</sub> samples show the best H<sub>2</sub> evolution activity.

6 Based on the results of the visible light photocatalytic performance and the structure  
7 characterizations of PtCo/g-C<sub>3</sub>N<sub>4</sub> nanosheet samples, a possible mechanism for photocatalytic H<sub>2</sub>  
8 evolution over PtCo/g-C<sub>3</sub>N<sub>4</sub> catalyst is proposed and illustrated in Fig. 12. Under visible light  
9 irradiation ( $\lambda \geq 400\text{nm}$ ), the polymeric g-C<sub>3</sub>N<sub>4</sub> absorbs photons and excites electron-hole pairs. However,  
10 the photo-generated charge carriers are likely to recombine without co-catalyst. The significant  
11 enhancement of H<sub>2</sub> evolution can be attributed to synergistic effect between g-C<sub>3</sub>N<sub>4</sub> and PtCo bimetallic  
12 NPs. After introducing PtCo NPs, the two materials closely bound together and form interfaces. The  
13 PtCo alloy NPs show higher electron capture capability and can stimulate electron transfer from g-C<sub>3</sub>N<sub>4</sub>  
14 towards PtCo NPs surface due to the lower Fermi level.<sup>45</sup> Moreover, the CB and VB edge potentials of  
15 polymeric g-C<sub>3</sub>N<sub>4</sub> are determined at -1.13 and +1.57 eV.<sup>46</sup> Therefore, in the PtCo/g-C<sub>3</sub>N<sub>4</sub> system, the  
16 photo-generated electrons in the CB of the g-C<sub>3</sub>N<sub>4</sub> transfer to PtCo co-catalysts via contacting interfaces,  
17 giving the conduction band electrons higher mobility and promoting the separation of electron-hole  
18 pairs. The holes in the VB of g-C<sub>3</sub>N<sub>4</sub> are consumed by TEOA sacrificial reagents. Therefore, the  
19 recombination process of the electron-hole pairs is effectively inhibited, resulting in obviously  
20 improvement of H<sub>2</sub> production for the PtCo/g-C<sub>3</sub>N<sub>4</sub> nanosheet photocatalysts.

21 To get more in-depth understanding of the electrical properties and the charge transfer process at  
22 g-C<sub>3</sub>N<sub>4</sub> and PtCo NPs interfaces, surface photovoltage spectroscopy (SPV) measurement was employed  
23 to reveal the kinetic behaviors of the photo-generated charge carriers in the PtCo/g-C<sub>3</sub>N<sub>4</sub> nanosheets.

1 The SPV survey could be beneficial for understanding the effect of PtCo NPs. Fig.13a illustrates the  
2 SPV spectra of g-C<sub>3</sub>N<sub>4</sub> and 1.0 wt% PtCo/g-C<sub>3</sub>N<sub>4</sub> nanosheets. The SPV signal ranging from 470-300nm  
3 is observed for pure g-C<sub>3</sub>N<sub>4</sub>. After loading PtCo NPs on the g-C<sub>3</sub>N<sub>4</sub> nanosheets, the sample shows  
4 obvious responses signal. The enhanced SPV signal intensity indicates that the introduction of PtCo  
5 NPs is beneficial to the separation of photo-generated electron-hole pairs in g-C<sub>3</sub>N<sub>4</sub> nanosheets. Fig.13b  
6 presents the corresponding phase spectroscopy of PtCo/g-C<sub>3</sub>N<sub>4</sub>, and the phase angles in the response  
7 region are in the range of +150 to +180 (470nm $\geq\lambda\geq$ 400nm). The phenomenon means that  
8 photo-generated electrons transfer from the g-C<sub>3</sub>N<sub>4</sub> to the PtCo NPs when equilibrium is reached in the  
9 PtCo/g-C<sub>3</sub>N<sub>4</sub> sample.<sup>47</sup> The PtCo/g-C<sub>3</sub>N<sub>4</sub> promotes the electron transfer from g-C<sub>3</sub>N<sub>4</sub> to PtCo, resulting  
10 in the accumulation of electrons on the PtCo NPs surface. More importantly, the SPV spectra are  
11 consistent with the results of photocatalytic H<sub>2</sub> evolution, which can explain the origin of enhanced  
12 separation efficiency of photo-generated electron-hole pairs in the PtCo/g-C<sub>3</sub>N<sub>4</sub> composites.

#### 13 4. Conclusions

14 In summary, PtCo NPs cocatalyst decorated ultrathin 2D g-C<sub>3</sub>N<sub>4</sub> nanosheet photocatalysts is  
15 successfully prepared with solvothermal synthesis approach. The doping of PtCo NPs does not affect  
16 the morphology and crystal structure of 2D g-C<sub>3</sub>N<sub>4</sub> nanosheets. The composite photocatalysts exhibited  
17 enhanced photocatalytic activity in the presence of small PtCo NPs. The optimal loading content of  
18 PtCo NPs was determined to be 1.0 wt% for g-C<sub>3</sub>N<sub>4</sub> nanosheets, and the corresponding H<sub>2</sub> production  
19 rate was 960  $\mu\text{mol}\cdot\text{h}^{-1}\cdot\text{g}^{-1}$ . A possible photocatalytic mechanism is proposed based on the experimental  
20 results. The surface photovoltage technique can be applied to investigate the photoelectric processes of  
21 PtCo/g-C<sub>3</sub>N<sub>4</sub>, leading to a better understanding of photocatalytic behavior to explore novel composite  
22 photocatalysts with advanced functions. Therefore, the PtCo NPs are a promising co-catalyst material

1 which can be potentially used for photocatalytic hydrogen evolution.

## 2 **Corresponding Author:**

3 E-mail: gelei@sina.com (Professor Lei Ge)

## 4 **Acknowledgements:**

5 This work was financially supported by the National Science Foundation of China (Grant No.  
6 21003157, 21273285 and 51572295), Beijing Nova Program (Grant No. 2008B76), and Science  
7 Foundation of China University of Petroleum, Beijing (Grant No. KYJJ2012-06-20).

## 8 **References**

- 9 1. P. V. Kamat, *J Phys Chem C*, 2007, **111**, 2834-2860.
- 10 2. M. Ni, M. K. H. Leung, D. Y. C. Leung and K. Sumathy, *Renew Sust Energ Rev*, 2007, **11**, 401-425.
- 11 3. V. Subramanian, E. E. Wolf and P. V. Kamat, *J Am Chem Soc*, 2004, **126**, 4943-4950.
- 12 4. A. Dawson and P. V. Kamat, *J Phys Chem B*, 2001, **105**, 960-966.
- 13 5. R. Asahi, T. Morikawa, T. Ohwaki, K. Aoki and Y. Taga, *Science*, 2001, **293**, 269-271.
- 14 6. J. Han, Z. Liu, K. Guo, X. Zhang, T. Hong and B. Wang, *Applied Catalysis B: Environmental*, 2015,  
15 **179**, 61-68.
- 16 7. T. T. Hong, Z. F. Liu, H. Liu, J. Q. Liu, X. Q. Zhang, J. H. Han, K. Y. Guo and B. Wang, *Journal Of*  
17 *Materials Chemistry A*, 2015, **3**, 4239-4247.
- 18 8. Z. F. Liu, K. Y. Guo, J. H. Han, Y. J. Li, T. Cui, B. Wang, J. Ya and C. L. Zhou, *Small*, 2014, **10**,  
19 3153-3161.
- 20 9. Z. W. Zhao, Y. J. Sun and F. Dong, *Nanoscale*, 2015, **7**, 15-37.
- 21 10. D. J. Martin, P. J. T. Reardon, S. J. A. Moniz and J. W. Tang, *J Am Chem Soc*, 2014, **136**,  
22 12568-12571.
- 23 11. Y. J. Zhang, T. Mori, L. Niu and J. H. Ye, *Energ Environ Sci*, 2011, **4**, 4517-4521.

- 1 12. X. C. Wang, K. Maeda, A. Thomas, K. Takanabe, G. Xin, J. M. Carlsson, K. Domen and M.  
2 Antonietti, *Nat Mater*, 2009, **8**, 76-80.
- 3 13. J. Y. Zhang, Y. H. Wang, J. Jin, J. Zhang, Z. Lin, F. Huang and J. G. Yu, *Acs Appl Mater Inter*, 2013,  
4 **5**, 10317-10324.
- 5 14. Y. Zheng, J. Liu, J. Liang, M. Jaroniec and S. Z. Qiao, *Energ Environ Sci*, 2012, **5**, 6717-6731.
- 6 15. J. Qin, S. Wang, H. Ren, Y. Hou and X. Wang, *Applied Catalysis B: Environmental*, 2015, **179**, 1-8.
- 7 16. S. C. Yan, Z. S. Li and Z. G. Zou, *Langmuir*, 2010, **26**, 3894-3901.
- 8 17. J. S. Zhang, M. W. Zhang, R. Q. Sun and X. C. Wang, *Angew Chem Int Edit*, 2012, **51**,  
9 10145-10149.
- 10 18. G. G. Zhang, J. S. Zhang, M. W. Zhang and X. C. Wang, *J Mater Chem*, 2012, **22**, 8083-8091.
- 11 19. J. Xu, L. W. Zhang, R. Shi and Y. F. Zhu, *Journal Of Materials Chemistry A*, 2013, **1**, 14766-14772.
- 12 20. S. B. Yang, Y. J. Gong, J. S. Zhang, L. Zhan, L. L. Ma, Z. Y. Fang, R. Vajtai, X. C. Wang and P. M.  
13 Ajayan, *Adv Mater*, 2013, **25**, 2452-2456.
- 14 21. X. D. Zhang, X. Xie, H. Wang, J. J. Zhang, B. C. Pan and Y. Xie, *J Am Chem Soc*, 2013, **135**, 18-21.
- 15 22. J. A. Singh, S. H. Overbury, N. J. Dudney, M. J. Li and G. M. Veith, *Acs Catal*, 2012, **2**, 1138-1146.
- 16 23. Y. J. Wang, R. Shi, J. Lin and Y. F. Zhu, *Energ Environ Sci*, 2011, **4**, 2922-2929.
- 17 24. X. Bai, R. Zong, C. Li, D. Liu, Y. Liu and Y. Zhu, *Applied Catalysis B: Environmental*, 2014, **147**,  
18 82-91.
- 19 25. X. L. Lu, K. Xu, P. Z. Chen, K. C. Jia, S. Liu and C. Z. Wu, *Journal Of Materials Chemistry A*, 2014,  
20 **2**, 18924-18928.
- 21 26. S. W. Cao and J. G. Yu, *J Phys Chem Lett*, 2014, **5**, 2101-2107.
- 22 27. J. Liu, Y. M. Yang, N. Y. Liu, Y. Liu, H. Huang and Z. H. Kang, *Green Chem*, 2014, **16**, 4559-4565.
- 23 28. X. W. Liu, D. S. Wang and Y. D. Li, *Nano Today*, 2012, **7**, 448-466.

- 1 29. R. T. Mu, Q. A. Fu, H. Xu, H. I. Zhang, Y. Y. Huang, Z. Jiang, S. O. Zhang, D. L. Tan and X. H. Bao,  
2 *J Am Chem Soc*, 2011, **133**, 1978-1986.
- 3 30. B. T. Sneed, A. P. Young, D. Jalalpoor, M. C. Golden, S. J. Mao, Y. Jiang, Y. Wang and C. K. Tsung,  
4 *Acs Nano*, 2014, **8**, 7239-7250.
- 5 31. C. C. Han, L. E. Wu, L. Ge, Y. J. Li and Z. Zhao, *Carbon*, 2015, **92**:31-40.
- 6 32. K. B. Vu, K. V. Bukhryakov, D. H. Anjum and V. O. Rodionov, *Acs Catal*, 2015, **5**, 2529-2533.
- 7 33. L. F. Liu, E. Pippel, R. Scholz and U. Gosele, *Nano Lett*, 2009, **9**, 4352-4358.
- 8 34. G. X. Chen, Y. Zhao, G. Fu, P. N. Duchesne, L. Gu, Y. P. Zheng, X. F. Weng, M. S. Chen, P. Zhang,  
9 C. W. Pao, J. F. Lee and N. F. Zheng, *Science*, 2014, **344**, 495-499.
- 10 35. Z. F. Hu and J. C. Yu, *Journal Of Materials Chemistry A*, 2013, **1**, 12221-12228.
- 11 36. X. Zhang, L. Z. Zhang, T. F. Xie and D. J. Wang, *J Phys Chem C*, 2009, **113**, 7371-7378.
- 12 37. L. Ge, C. C. Han and J. Liu, *J Mater Chem*, 2012, **22**, 11843-11850.
- 13 38. L. Ge, C. C. Han and J. Liu, *Appl Catal B-Environ*, 2011, **108**, 100-107.
- 14 39. C. C. Han, L. Ge, C. F. Chen, Y. J. Li, X. L. Xiao, Y. N. Zhang and L. L. Guo, *Appl Catal B-Environ*,  
15 2014, **147**, 546-553.
- 16 40. L. Ge, C. C. Han, X. L. Xiao and L. L. Guo, *Appl Catal B-Environ*, 2013, **142**, 414-422.
- 17 41. B. Y. Xia, H. B. Wu, N. Li, Y. Yan, X. W. Lou and X. Wang, *Angew Chem Int Ed*, 2015, **54**,  
18 3797-3801.
- 19 42. D. S. Wang and Y. D. Li, *Adv Mater*, 2011, **23**, 1044-1060.
- 20 43. M. N. Cao, D. S. Wu and R. Cao, *Chemcatchem*, 2014, **6**, 26-45.
- 21 44. H. Z. Yang, J. Zhang, K. Sun, S. Z. Zou and J. Y. Fang, *Angew Chem Int Ed*, 2010, **49**, 6848-6851.
- 22 45. S. Huang, Q. He, J. Zai, M. Wang, X. Li, B. Li and X. Qian, *Chem Commun*, 2015, **51**, 8950-8953.
- 23 46. L. Ge, C. C. Han, X. L. Xiao, L. L. Guo and Y. J. Li, *Mater Res Bull*, 2013, **48**, 3919-3925.

- 1 47. T. F. Jiang, T. F. Xie, Y. Zhang, L. P. Chen, L. L. Peng, H. Y. Li and D. J. Wang, *Phys Chem Chem*
- 2 *Phys*, 2010,**12**: 15476-15481.

3

1 **Figure Captions:**

2 **Fig.1.** Schematic illustration of the formation route to PtCo/g-C<sub>3</sub>N<sub>4</sub> photocatalysts (Bulk and  
3 nanosheets).

4 **Fig.2.** XRD patterns of PtCo/g-C<sub>3</sub>N<sub>4</sub> nanosheet photocatalysts, as well as of the pure PtCoX (X=0, 1, 3).

5 **Fig.3.** UV-vis diffuse reflectance of PtCo<sub>x</sub>/g-C<sub>3</sub>N<sub>4</sub> composite samples.

6 **Fig.4.** The HRTEM images with different magnifications for the 1.0 wt% PtCo/g-C<sub>3</sub>N<sub>4</sub> nanosheet  
7 photocatalysts.

8 **Fig.5.** XPS spectra of PtCo/g-C<sub>3</sub>N<sub>4</sub> sample: (a) C 1s; (b) N 1s; (c) Pt 4f (Pt/Pt<sub>3</sub>Co/PtCo/PtCo<sub>3</sub>); (d) Co  
9 2p.

10 **Fig.6.** Photocatalytic H<sub>2</sub> evolution over the bulk PtCo<sub>x</sub>/g-C<sub>3</sub>N<sub>4</sub> composite samples with different Pt/Co  
11 percentage in the same 1wt% content.

12 **Fig.7.** Photocatalytic H<sub>2</sub> evolution over the PtCo<sub>x</sub>/g-C<sub>3</sub>N<sub>4</sub> nanosheet composite samples with different  
13 Pt/Co percentage in the same 1.0 wt%.

14 **Fig.8.** The H<sub>2</sub> evolution rate over different bulk and nanosheet samples.

15 **Fig.9.** Photocatalytic H<sub>2</sub> evolution over PtCo/g-C<sub>3</sub>N<sub>4</sub> nanosheet samples with different PtCo contents  
16 under visible light irradiation.

17 **Fig.10.** Cycling runs for the photocatalytic hydrogen evolution in the presence of 1.0 wt% PtCo/g-C<sub>3</sub>N<sub>4</sub>  
18 nanosheet sample under visible light illumination ( $\lambda \geq 400\text{nm}$ ).

**Fig.11.** The schematic illustration of photo-excited electron injection from CB of g-C<sub>3</sub>N<sub>4</sub> to the PtCo  
NPs and Pt NPs.

19 **Fig.12.** The schematic illustration for electron charge transfer and H<sub>2</sub> evolution mechanism under  
20 visible light irradiation.

21 **Fig.13.** SPV spectra of pure g-C<sub>3</sub>N<sub>4</sub> and 1wt% PtCo/g-C<sub>3</sub>N<sub>4</sub>: (a) Photovoltage; (b) Phase.

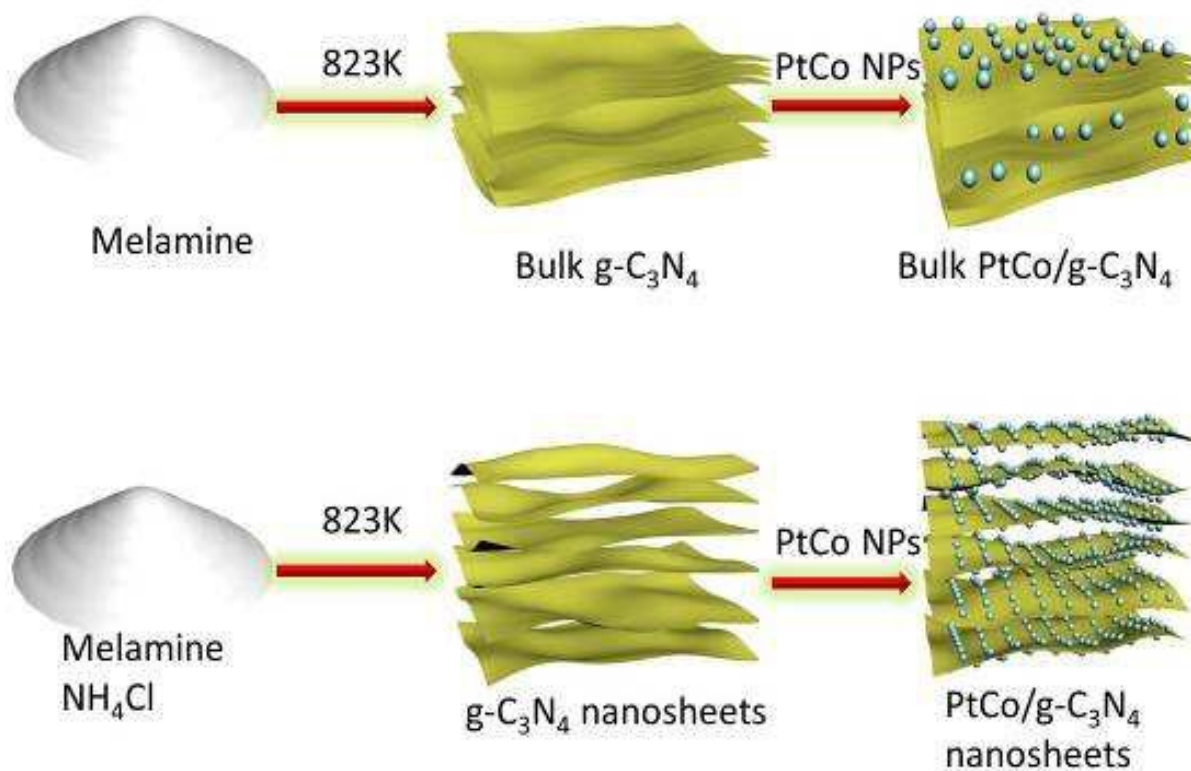


**Fig.1.** Schematic illustration of the formation route to PtCo/g-C<sub>3</sub>N<sub>4</sub> photocatalysts (Bulk and nanosheets).

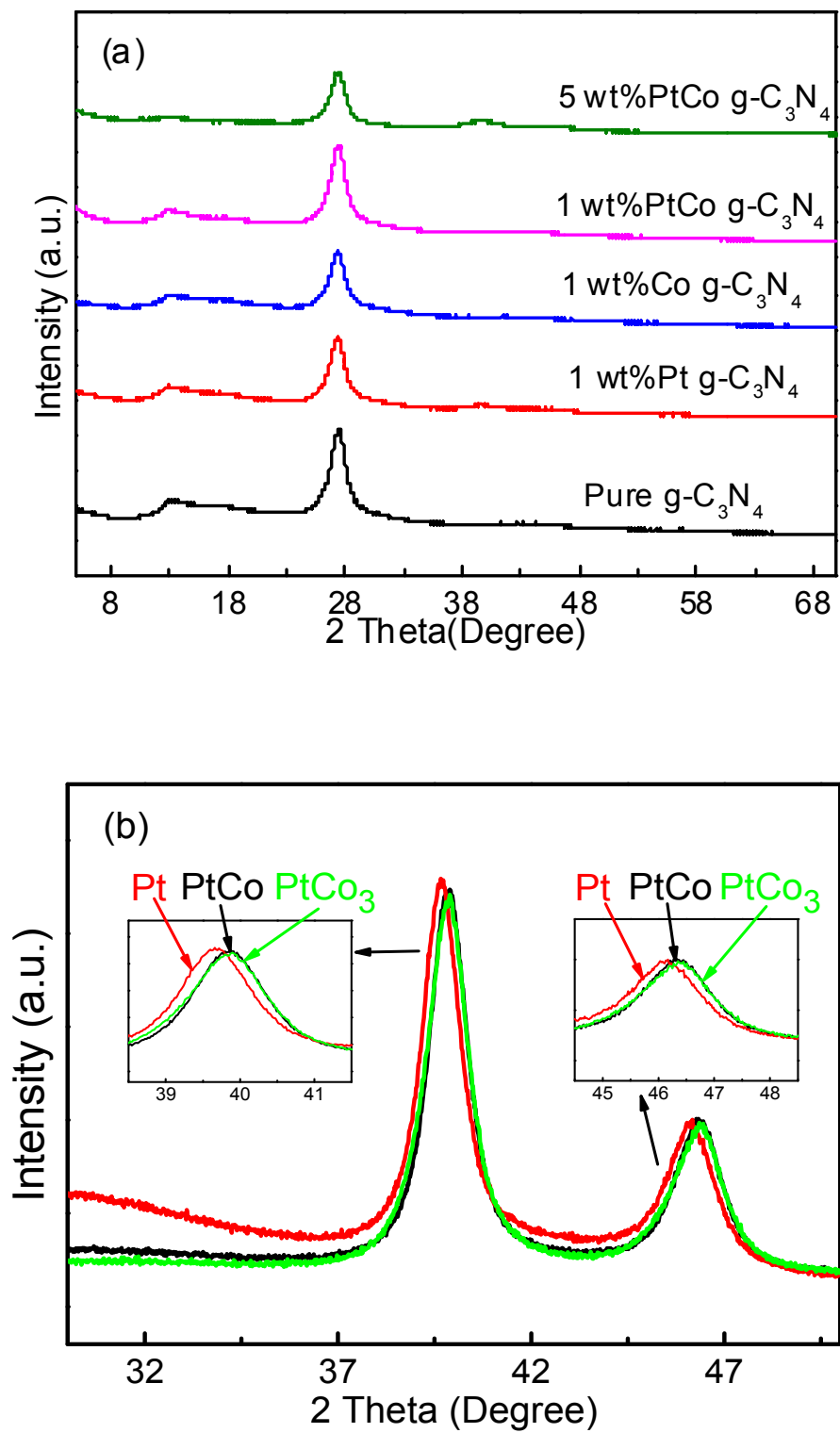


**Fig.2.** XRD patterns of PtCo/g-C<sub>3</sub>N<sub>4</sub> nanosheet photocatalysts, as well as of the pure PtCo<sub>X</sub> (X=0, 1, 3)

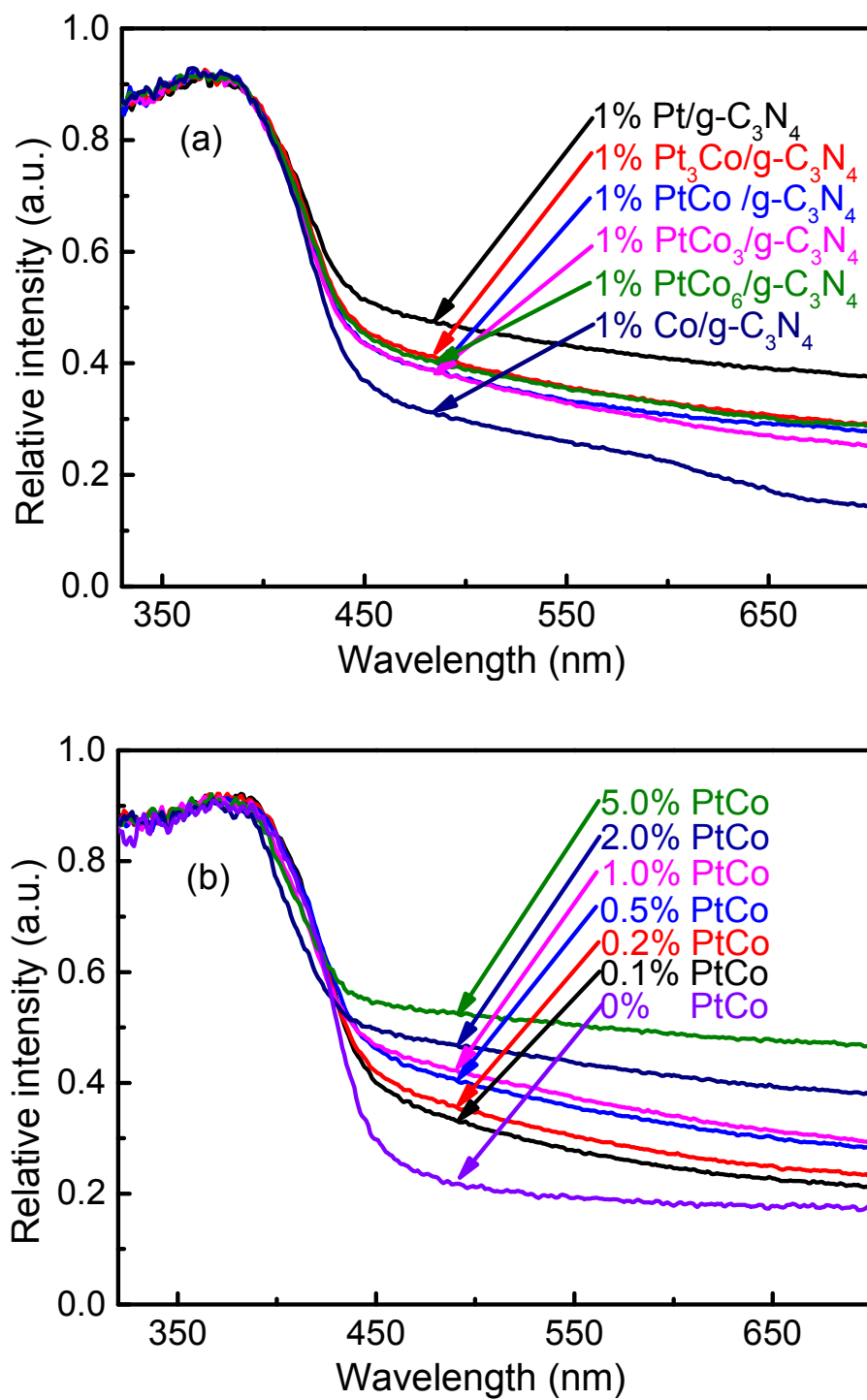
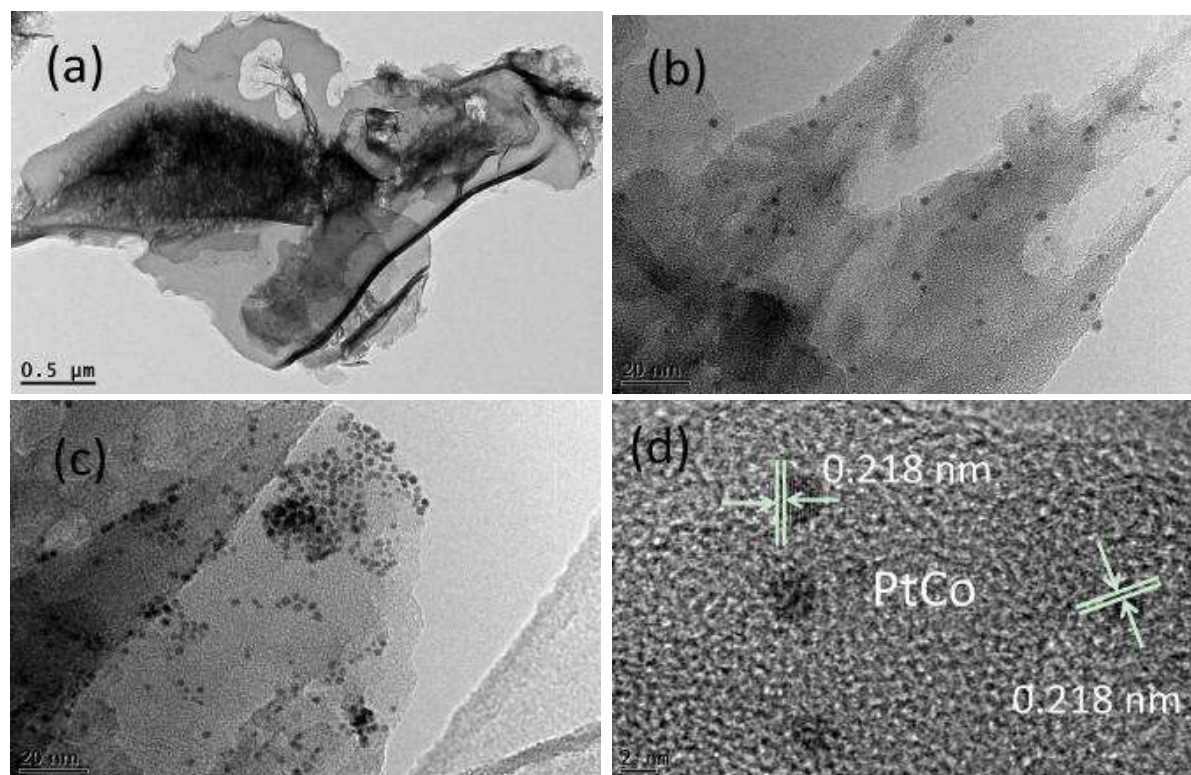
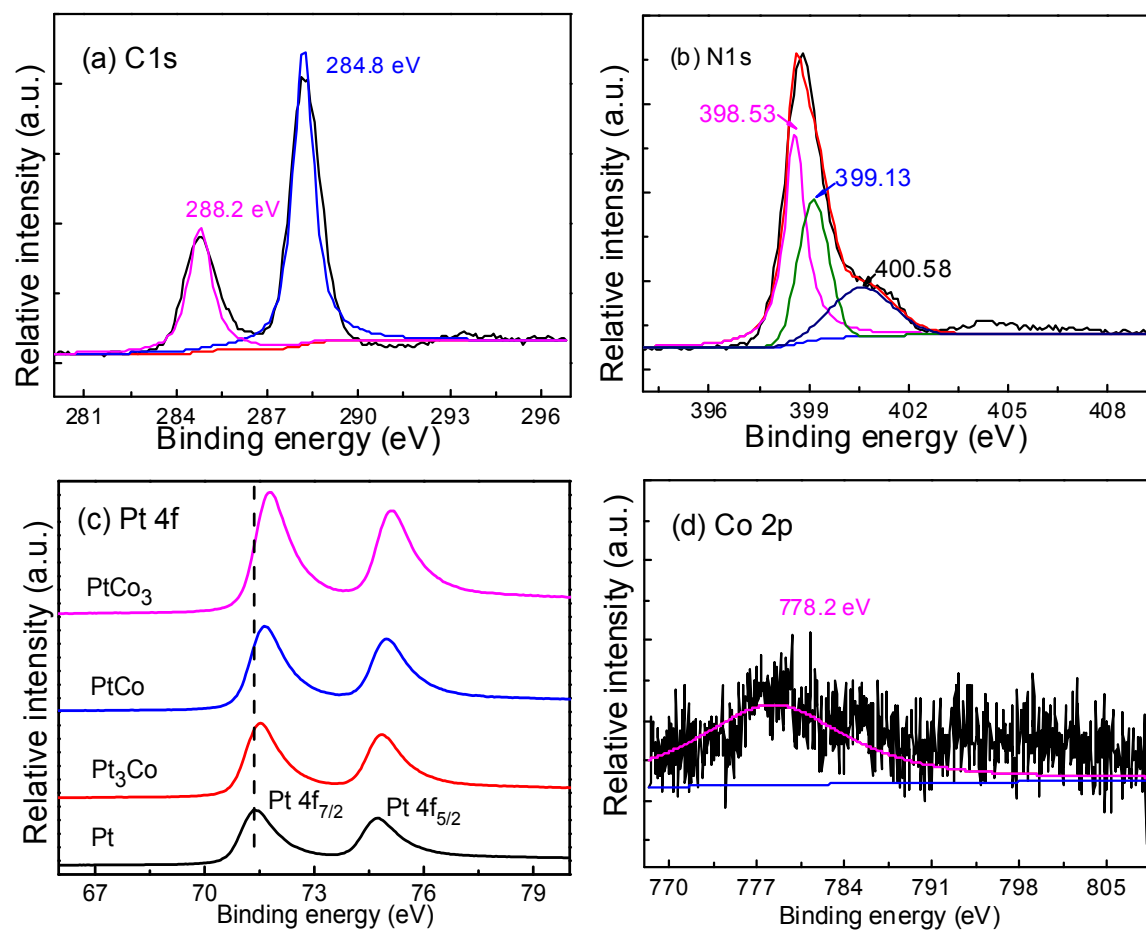


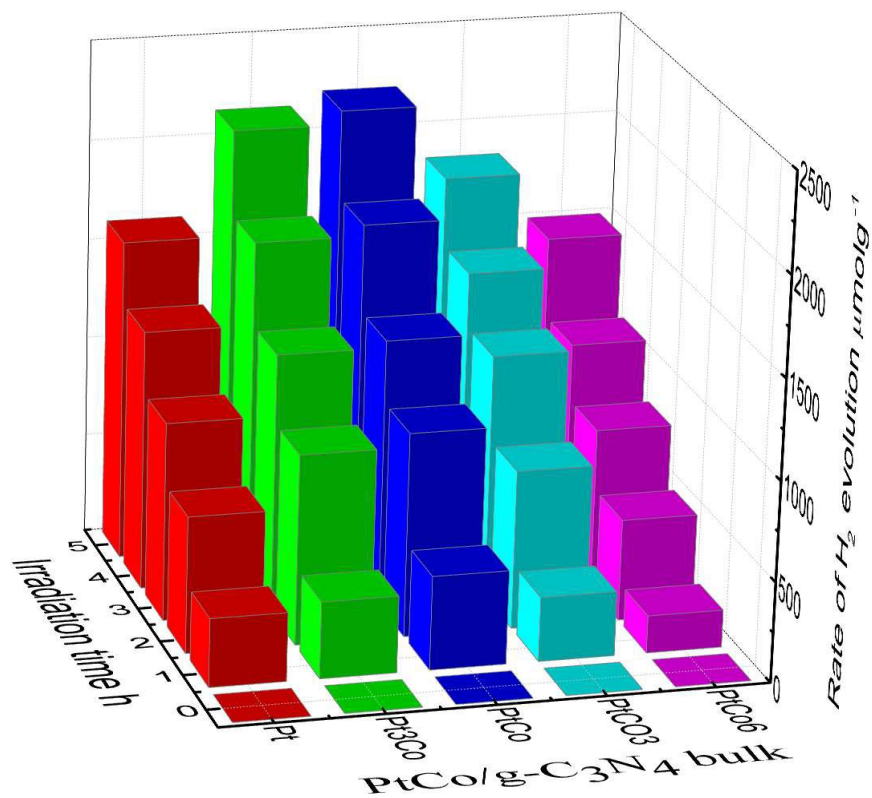
Fig.3. UV-vis diffuse reflectance of PtCox/g-C<sub>3</sub>N<sub>4</sub> composite samples.



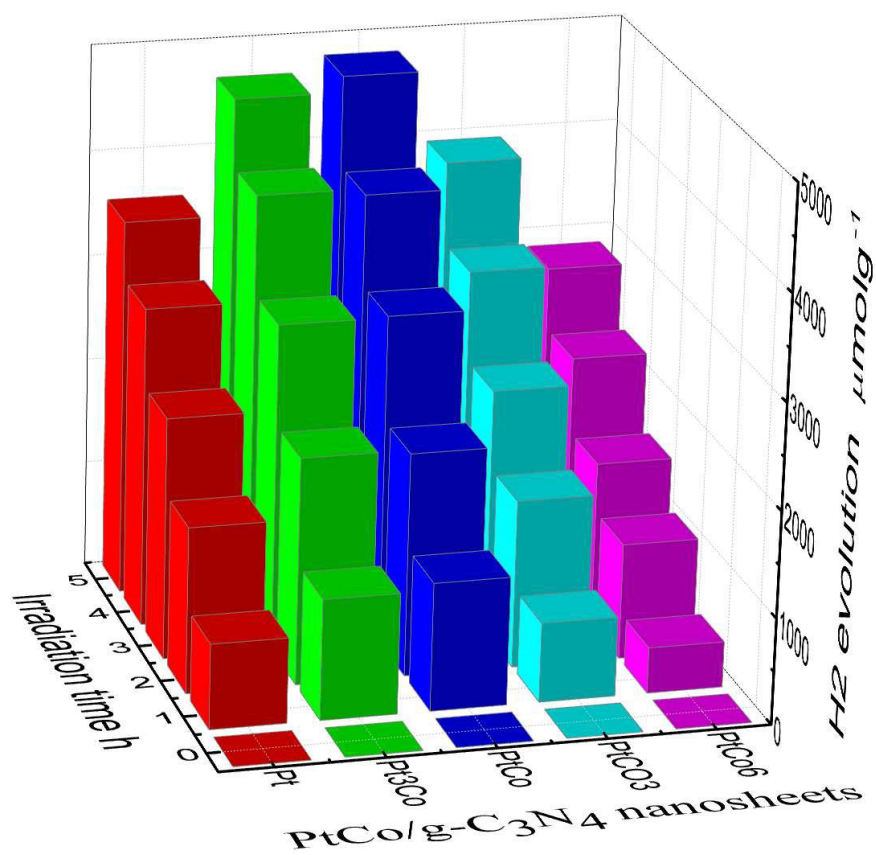
**Fig.4.** The HRTEM images with different magnifications for the 1.0 wt% PtCo/g-C<sub>3</sub>N<sub>4</sub> nanosheet photocatalysts.



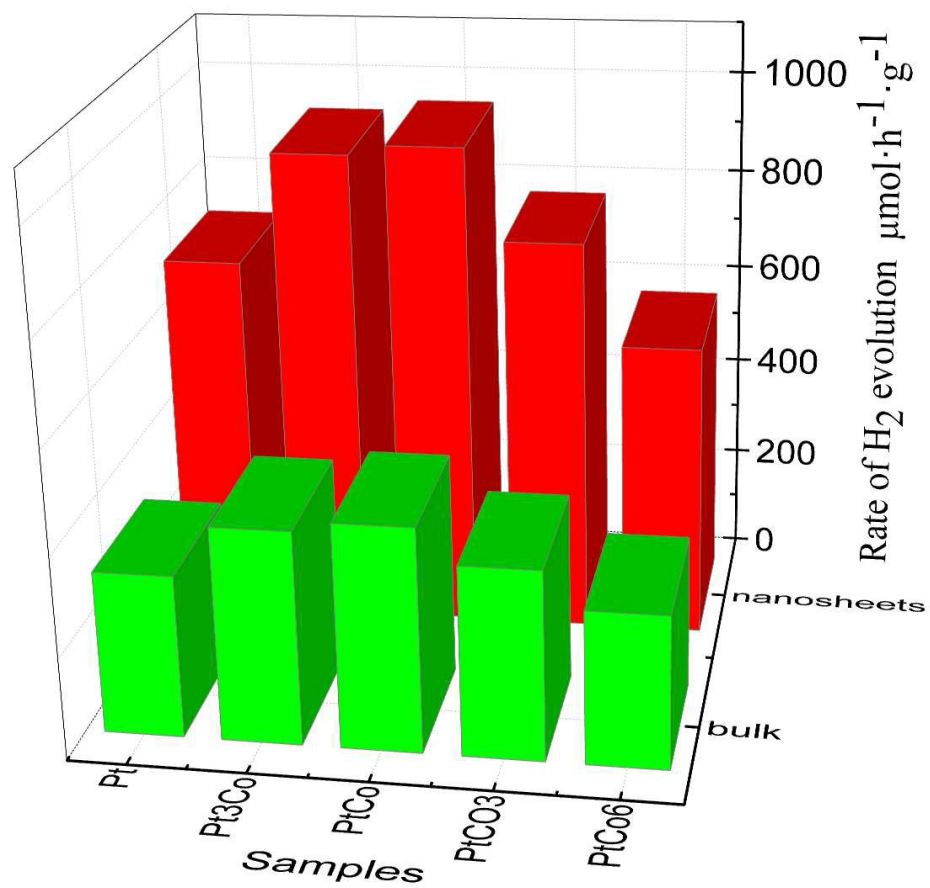
**Fig.5.** XPS spectra of PtCo/g-C<sub>3</sub>N<sub>4</sub> sample: (a) C 1s; (b) N 1s; (C) Pt 4f (Pt/Pt<sub>3</sub>Co/PtCo/PtCo<sub>3</sub>); (d) Co 2p.



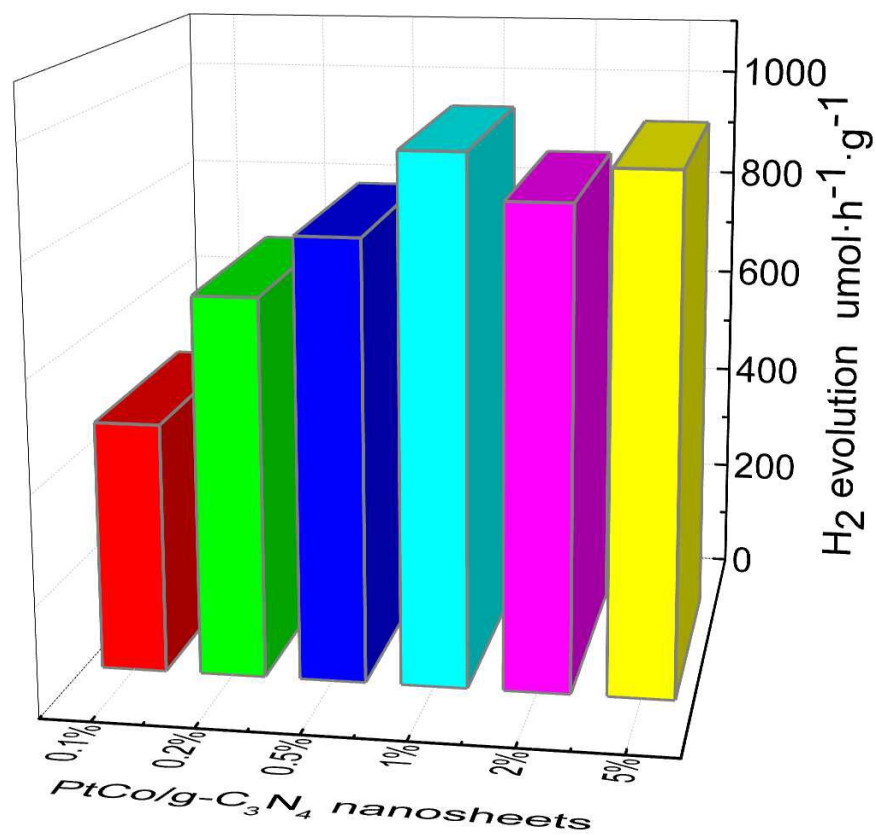
**Fig.6.** Photocatalytic H<sub>2</sub> evolution over the bulk PtCo<sub>x</sub>/g-C<sub>3</sub>N<sub>4</sub> composite samples with different Pt/Co percentage in the same 1wt% content.



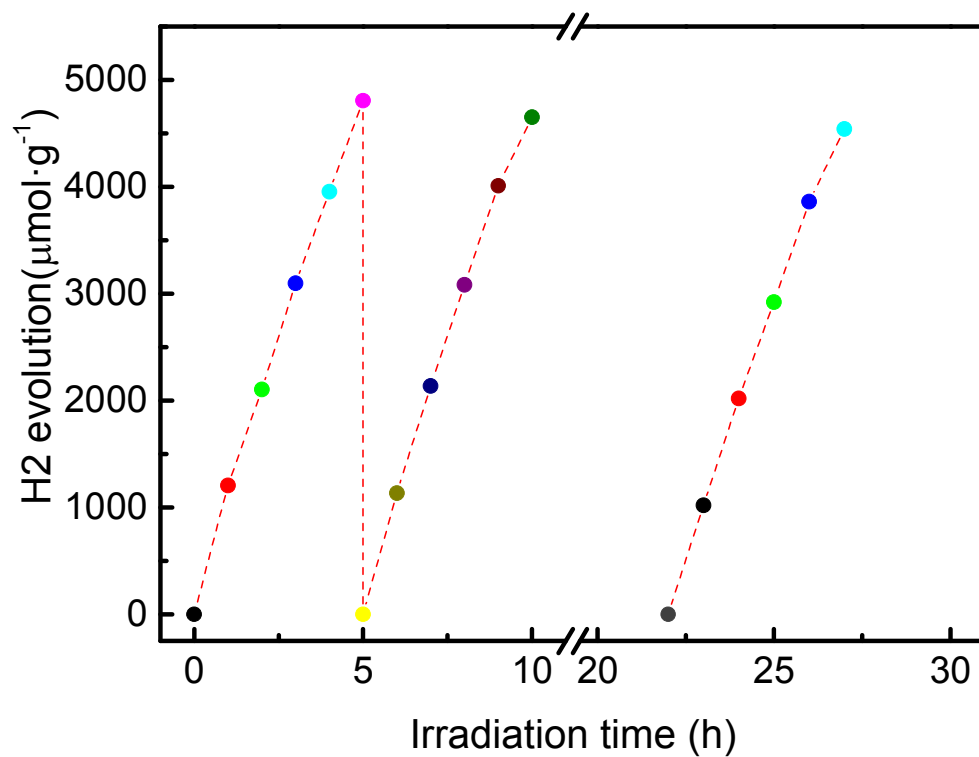
**Fig.7.** Photocatalytic H<sub>2</sub> evolution over the PtCox/g-C<sub>3</sub>N<sub>4</sub> nanosheet composite samples with different Pt/Co percentage in the same 1.0 wt%.



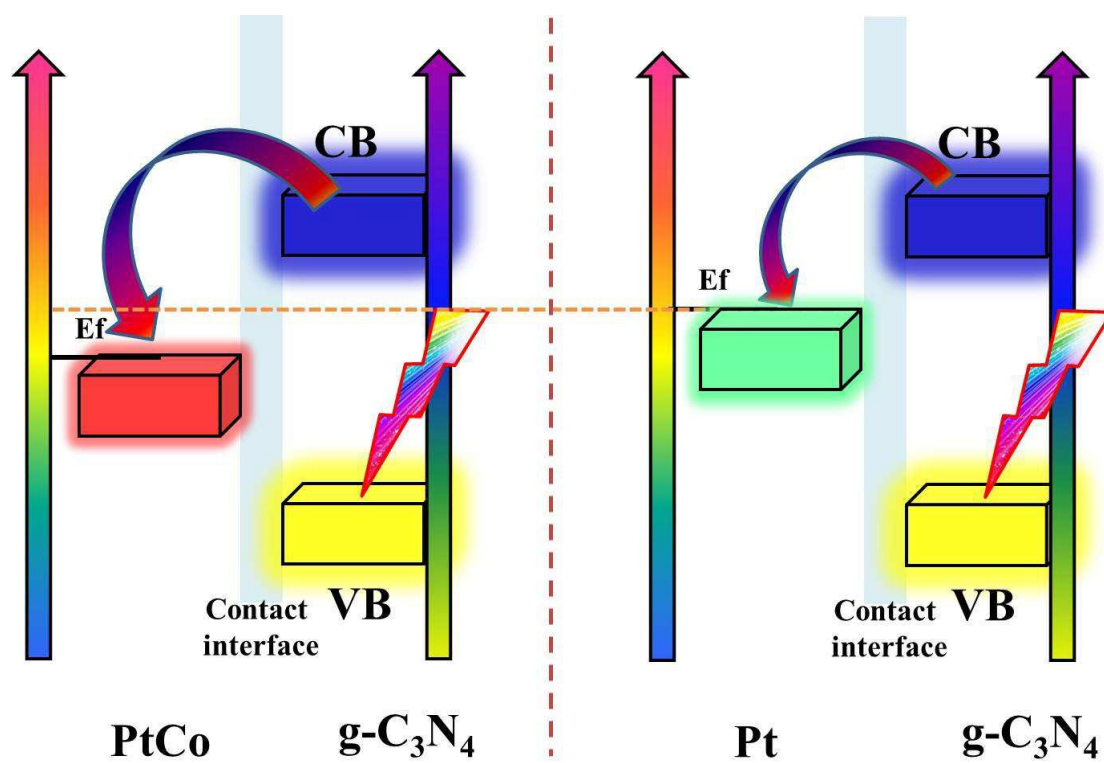
**Fig .8.** The H<sub>2</sub> evolution rate over different bulk and nanosheet samples.



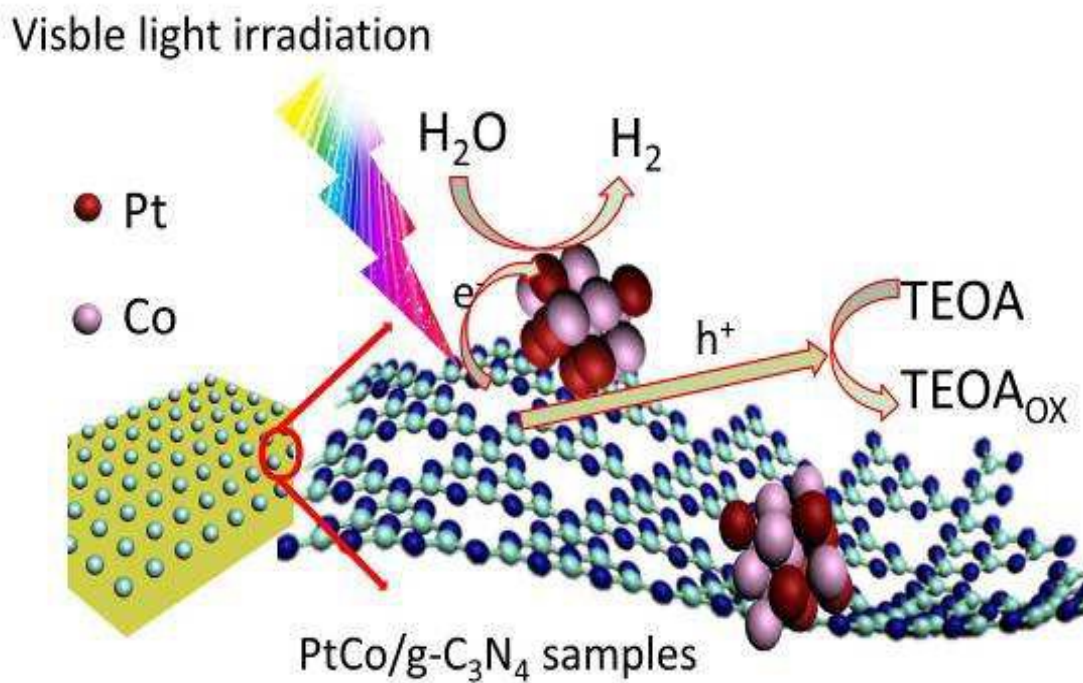
**Fig.9.** Photocatalytic H<sub>2</sub> evolution over PtCo/g-C<sub>3</sub>N<sub>4</sub> nanosheet samples with different PtCo contents under visible light irradiation.



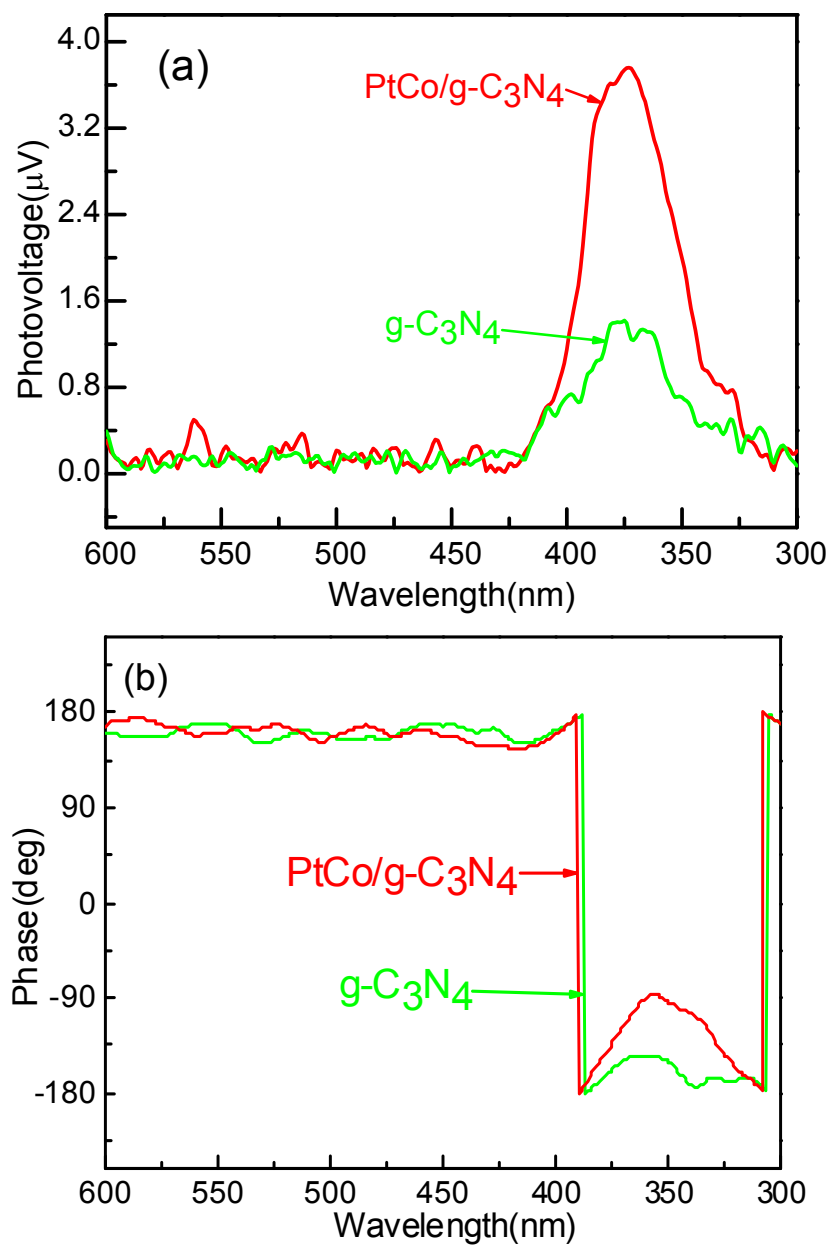
**Fig.10.** Cycling runs for the photocatalytic hydrogen evolution in the presence of 1.0 wt% PtCo/g-C<sub>3</sub>N<sub>4</sub> nanosheet sample under visible light illumination ( $\lambda \geq 400\text{nm}$ ).



**Fig.11.** The schematic illustration of photo-excited electron injection from CB of g-C<sub>3</sub>N<sub>4</sub> to the PtCo NPs and Pt NPs.

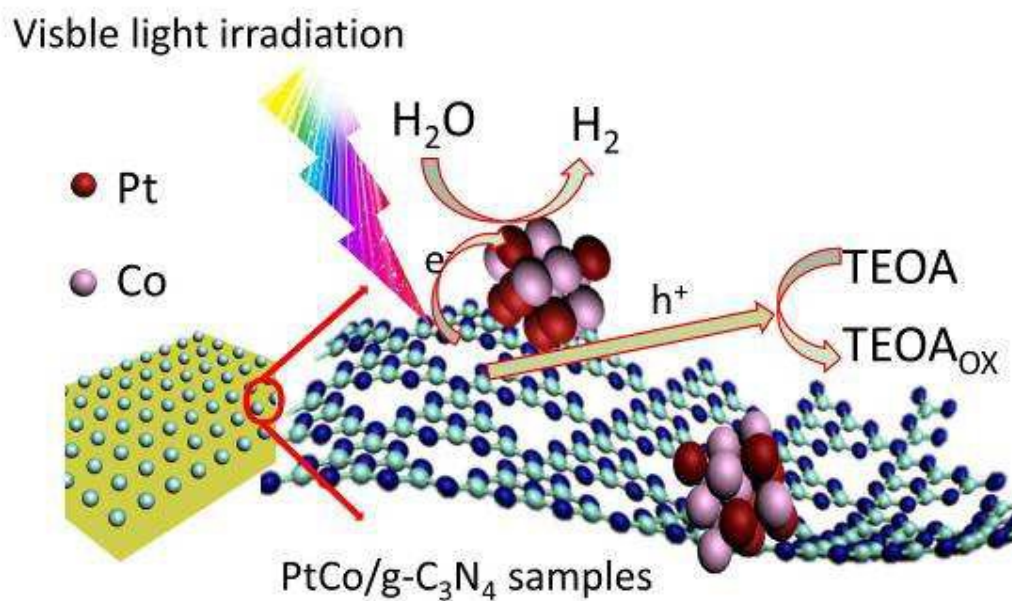


**Fig.12.** The schematic illustration for electron charge transfer and H<sub>2</sub> evolution mechanism under visible light irradiation.



**Fig.13.** SPV spectra of pure g-C<sub>3</sub>N<sub>4</sub> and 1wt% PtCo/g-C<sub>3</sub>N<sub>4</sub>: (a) Photovoltage; (b) Phase.

## Graphical Abstract



Novel PtCo/g-C<sub>3</sub>N<sub>4</sub> nanosheets with efficient visible light induced photocatalytic activity for H<sub>2</sub> evolution.